Available online at www.sciencedirect.com

SciVerse ScienceDirect

Ceramics International 39 (2013) 5197–5203

CERAMICS INTERNATIONAL

www.elsevier.com/locate/ceramint

# Synthesis of N-doped ZnO nanoparticles with improved photocatalytical activity

Shibin Sun[a,c], Xueting Chang[b,*], Xiujuan Li[c], Zhenjiang Li[c]

[a]College of Logistics Engineering, Shanghai Maritime University, Shanghai 200135, People's Republic of China
[b]Institute of Marine Materials Science and Engineering, Shanghai Maritime University, Shanghai 200135, People's Republic of China
[c]College of Electromechanical Engineering, Qingdao University of Science and Technology, Qingdao 266061, China

Received 26 November 2012; received in revised form 5 December 2012; accepted 5 December 2012
Available online 20 December 2012

**Abstract**

ZnO nanoparticles with diameters of 20–50 nm were initially prepared by solvothermal route using $ZnCl_2$ and ethylene glycol as raw materials. With the as-prepared ZnO nanoparticles as precursor and melamine as N source, N-doped ZnO nanoparticles were then successfully obtained by a simple, efficient, and environmentally-friendly vacuum atmosphere method. Both the undoped and N-doped ZnO nanoparticles have been characterized by X-ray diffraction, scanning electron microscopy, transmission electron microscopy, and X-ray photoelectron spectrometry. The N-doped ZnO nanoparticles were found to exhibit obviously improved photocatalytic performance for the degradation of methyl orange under simulated daylight irradiation in comparison with the undoped ZnO nanoparticles. The extending light absorption towards the visible-light region and increased crystallinity of the N-doped ZnO nanoparticles contribute equally to the improved photocatalytic performance. The present vacuum atmosphere method opens up a new strategy for preparing other N-doped oxide semiconductors such as $TiO_2$.


*Keywords:* B. Electron microscopy; C. Optical properties; E. Functional applications; Powders: chemical reaction

## 1. Introduction

Oxide semiconductors are important for many environmental and energy issues, because they can utilize solar energy to eliminate harmful pollutants present in air and water [1–4]. Since the discovery of water splitting by $TiO_2$, a wide range of research has been carried out on various oxide semiconductor photocatalysts including ZnO [5–7], $TiO_2$ [8–10], $WO_3$ [11–13], $In_2O_3$ [14], and $SnO_2$ [15], with emphasis on understanding the fundamental photocatalytic mechanism, enhancing the photocatalytic activity, and widening the scope of applications. Among various functional oxide semiconductors, ZnO is biocompatible, biodegradable, nontoxic, and highly stable, making it more competitive than other semiconducting oxide photocatalysts for environmental applications [16–20]. However, the photocatalytic efficiency of ZnO is still not high enough for practical application due to its wide bandgap (3.37 eV) and the rapid recombination of photoexcited electron-hole pairs [21–22].

Doping of other elements in suitable manner could extend the light absorption of ZnO from the ultraviolet (UV) to the visible region by narrowing its bandgap and is found to be an effective route to enhance its photocatalytic performance. Cation doping usually produces additional defects or impurities in ZnO, which could act as recombination centers of photoexcited electron-hole pairs and deteriorate the photocatalytic activity [23]. In contrast, anion elements with small radii are promising candidates for doping because they could be easily incorporated into the lattice of ZnO by replacing the O atoms or occupying the interstitial sites. For example, both the N- and S-doped ZnO exhibited enhanced photocatalytic activity for the degradation of organic pollutants compared to that of pure ZnO under solar light irradiation [24,25]. N-doping of

*Corresponding author. Tel.: +86 21 3828 2611.
*E-mail address:* xuetingchang@yahoo.cn (X. Chang).

0272-8842/$ - see front matter © 2012 Elsevier Ltd and Techna Group S.r.l. All rights reserved.
http://dx.doi.org/10.1016/j.ceramint.2012.12.018

ZnO nanotetrapods and ZnO nanowire arrays could also significantly enhanced their light harvesting in the visible-light region, making them potential photoelectrochemical cells for water splitting [26,27]. Up till now, various strategies have been developed for the doping of anion elements in ZnO, such as spray pyrolysis, combustion technique, thermal evaporation, as well as the commonly-used thermal nitridation route with ammonia as N source [22,24,27–29]. These reported methods require either high temperature or complex procedures or toxic N source and cannot therefore be appropriate for the practical application. The search for simple and environmental strategies for preparing anion elements-doped ZnO still remains a challenge and is of great importance.

In this paper, we present a simple vacuum atmosphere method to synthesize the N-doped ZnO nanoparticles (N–ZnO NPs) with ZnO nanoparticles (NPs) and melamine as precursors without introducing external N source. At the end of the doping process, the melamine could be reversibly obtained in the furnace tube and no harmful by-product remained, making the present method environmentally friendly. The N–ZnO NPs were found to exhibit obviously improved photocatalytic performance in comparison with the undoped ZnO NPs. The present vacuum atmosphere method shows versatility in preparing other N-doped oxide semiconductors such as $TiO_2$.

## 2. Experimental details

### 2.1. Preparation of ZnO NPs

ZnO NPs were prepared by a simple solvothermal route. Generally, 1.5 mmol of $ZnCl_2$ was firstly dissolved in 2 ml of ethanol in a beaker to obtain a solution. Then, 1.5 mmol of NaOH was added to the solution, which was subsequently transferred into a Teflon-lined high-pressure reaction vessel of 100 mL capacity. 60 ml of ethylene glycol were added to the vessel with the precursor solution. The reaction vessel was finally sealed and heated at 200 °C in a Muffle furnace for 24 h. After natural cooling to room temperature, the as-synthesized products were washed thoroughly with distilled water several times, and finally centrifuged with distilled water, ethanol and acetone, respectively.

### 2.2. Preparation of N-doped ZnO NPs

N–ZnO NPs was prepared by a vacuum atmosphere method in a vacuum tube furnace. The as-synthesized ZnO NPs were firstly mixed with melamine with a weight ratio of 1:1 by ball milling. The mixture was dispersed on a quartz plate, which was then located in the central region of the tube furnace. Before heating, the furnace chamber was purged using a rotary vacuum pump for 30 min to receive a certain degree of vacuum. The furnace was subsequently heated at 380 °C for 2 h to finish the reaction. Finally, the furnace was cooled down to room temperature and the powders were collected for further examination. N-doped $TiO_2$ (N–$TiO_2$) NPs were also synthesized by the same method with $TiO_2$ NPs as precursor.

### 2.3. Characterization

The crystalline structure, morphology, chemical composition and surface features of the as-synthesized products were characterized by X-ray diffraction (XRD, D/MAX-2500, Cu radiation), energy dispersive X-ray spectroscopy (EDS), transmission electron microscopy (TEM, JEOL 2000FX, operated at 120 kV), high magnification transmission electron microscopy (HRTEM, JEOL JEM 2100, operated at 200 kV) and X-ray photoelectron spectrometry (XPS, PHI 5300, Mg kR X-ray source, 1253.6 eV).

### 2.4. Photocatalytic tests

For the photocatalytic evaluation, methyl orange (MO) was adopted as typical pollutant. The degradation of MO by ZnO and N–ZnO NPs was carried out in a photochemical reactor containing a suspension of the photocatalysts (20 mg) in an MO aqueous solution (50 ml, 10 mg/L) with continuing agitation using a magnetic stirrer. Simulated daylight irradiation was provided by a 350 W Xe lamp. Prior to the light irradiation, the MO solutions with the photocatalysts were kept in dark for 2 h to reach an adsorption–desorption equilibrium. The absorbance of MO solutions before and after the photocatalytic degradation by the photocatalysts was analyzed by UV–vis diffuse reflectance spectroscopy (U-3010, HITACHI). The concentration of MO in aqueous solution was determined by the maximum absorption measurement (around 465 nm of wavelength). The photocatalytic efficiencies of MO over different photocatalysts are defined by the equation of $((C_0-C)/C_0) \times 100\%$, where $C$ is the concentration of MO aqueous solution after light irradiation, and $C_0$ is the equilibrium concentration of MO at the equilibrium adsorption state. For comparison, photocatalytic properties of $TiO_2$ and N-doped $TiO_2$ NPs were also studied.

## 3. Results and discussions

Fig.1a shows the XRD pattern of the solvothermally-synthesized sample with $ZnCl_2$ as precursor. All the diffraction peaks could be indexed to hexagonal wurtzite structure of ZnO (JCPD no. 36-1451), proving that the resulting sample are pure ZnO. It is obvious that the (100), (002) and (101) planes possess the highest intensities, indicative of anisotropic growth of the as-prepared ZnO. The XRD pattern of the N–ZnO is shown in Fig. 1b. The diffraction peaks are also in good agreement with those of hexagonal ZnO (JCPDS card 36-1451) and are almost identical to that of the pure ZnO, indicating that the N atoms has been doped in the ZnO crystal and no new phase was formed. Compared to that of the pure

ZnO, interestingly, the diffraction peaks of the N–ZnO became sharper and narrower, revealing increased size and improved crystallinity.

Fig. 2a is a SEM image of the solvothermally-synthesized ZnO, which reveals that the ZnO are composed of NPs with diameters of 20–50 nm. TEM image of the ZnO NPs indicates that they exhibit semi-spherical morphology and are agglomerated, as shown in Fig. 2b. HRTEM image (Fig. 2c) demonstrates that the ZnO NPs are structurally uniform and are adhered to each other with clean and clear interface. The lattice spacing is measured to be 0.25 nm, corresponding to the (101) plane of the hexagonal ZnO. The SAED pattern (Fig. 2e) recorded in Fig. 2c exhibits bright spots, indicating that the ZnO NPs are single crystalline. Fig. 2d shows a typical SEM image of the as-prepared N–ZnO NPs, which presents similar morphology to that of the pure ZnO NPs. Notably, however, the ZnO NPs have been further agglomerated after the N-doping process, leading to the formation of larger particle. The fine feature of the ZnO NPs, compared with their corresponding bulk form, make them more likely to absorb ambient energy upon heating. In this work, agglomeration of the ZnO NPs within small range only occurs due to the low reaction temperature and short reaction period.

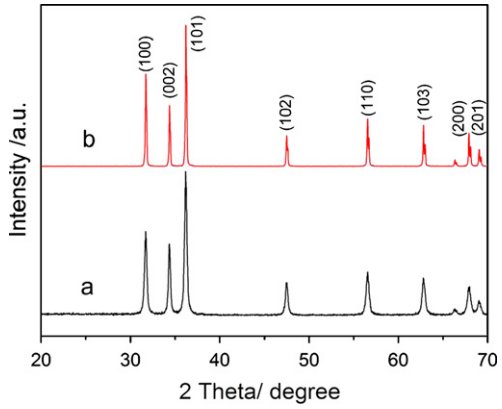


Fig. 1. XRD patterns of (a) ZnO and (b) N–ZnO NPs.

The surface compositions of the ZnO NPs and the N–ZnO NPs are investigated by XPS analysis and the corresponding XPS spectra are shown in Fig. 3. The carbon peak (C 1s) at 285 eV is due to the carbon paste used to stick the samples on the mount. From Fig. 3a, it is clear that all the peaks of the ZnO NPs are ascribed to Zn, O, and C elements, and no peaks characteristic of impurities are observed. As for the N–ZnO NPs (Fig. 3b), a small amount of N could be detected, evidencing the presence of N in the N–ZnO NPs. Fig. 3c provides the N

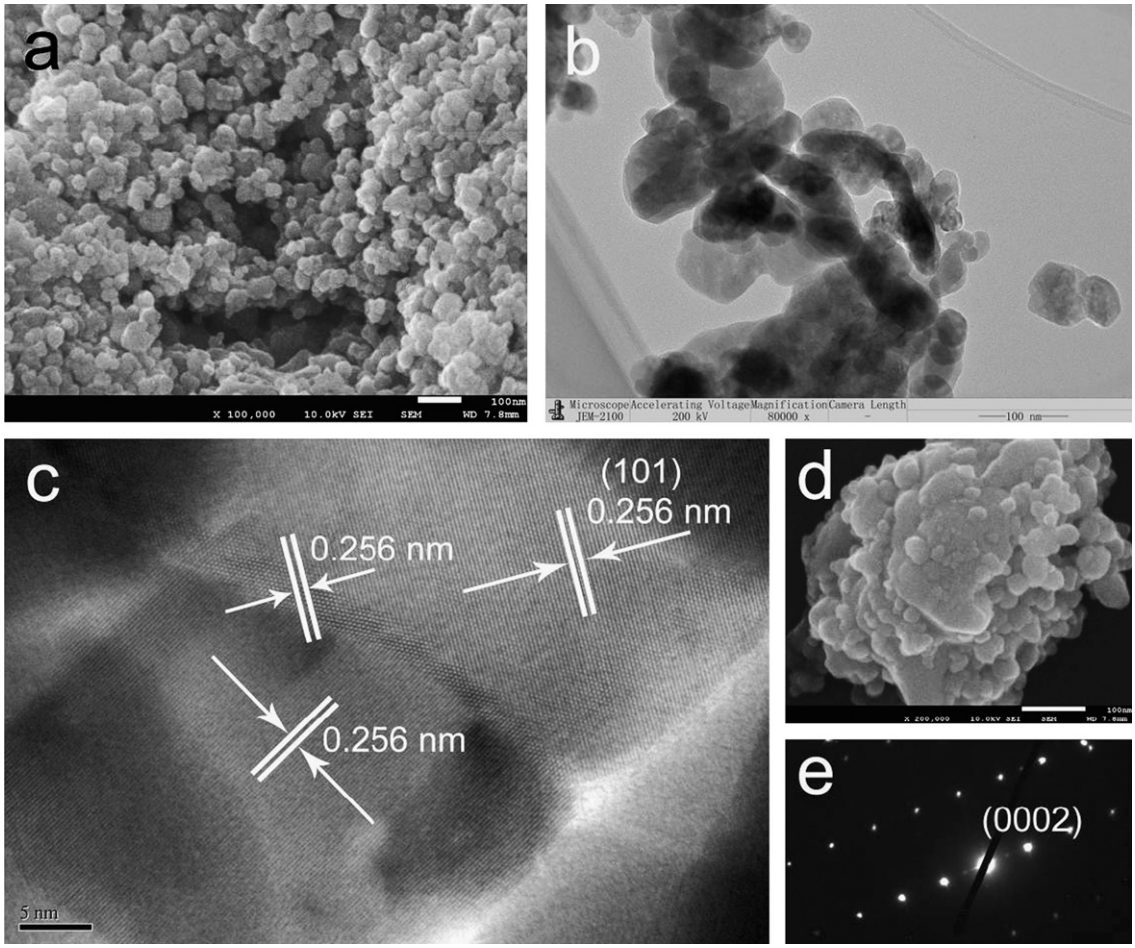


Fig. 2. (a) SEM, (b) TEM, and (c) HRTEM images of ZnO NPs; (d) SEM image of N–ZnO NPs; and (e) the corresponding SAED pattern from Fig. 1c.

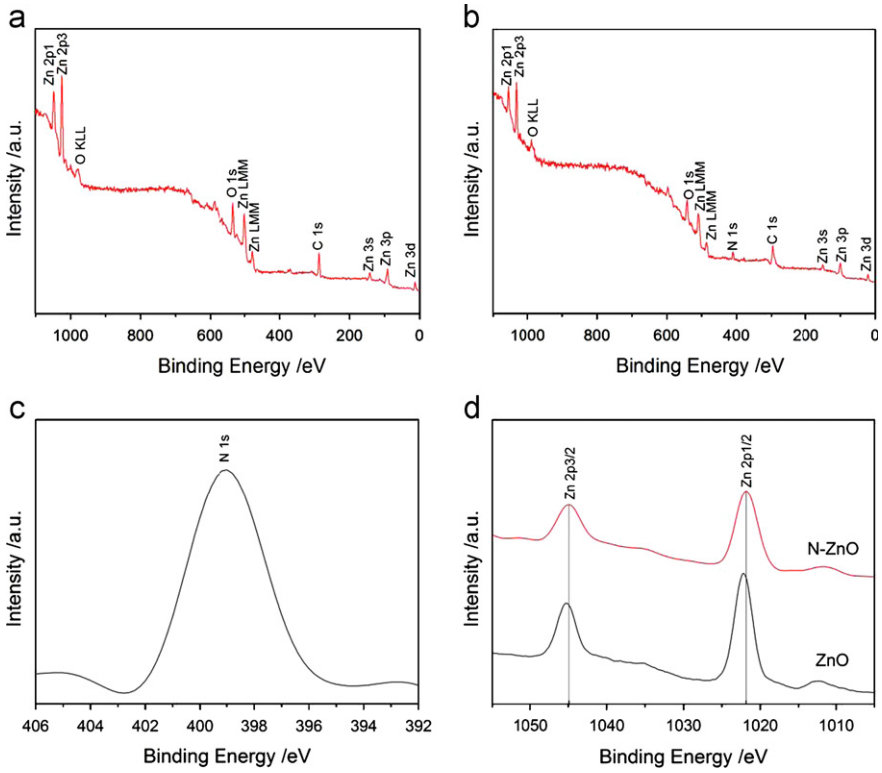


Fig. 3. XPS survey spectra of (a) ZnO and (b) N–ZnO NPs; (c) N 1s core-level spectrum; and (d) Zn 2p core-level spectra for ZnO and N–ZnO NPs.

1s core level of the N–ZnO NPs. One peak of binding energy at about 400 eV can be observed, which is attributed to the presence of Zn–N bond. EDS result (see Supplementary material) further proves the doping of N atoms in the ZnO NPs. Additionally, the ICP-AES results indicate that the doping amount of N in the N–ZnO NPs is about 0.8 wt%. The Zn 2p core-level spectra for both the ZnO and the N–ZnO NPs are shown in Fig. 3d. For the pure ZnO NPs, the peak positions at 1021.45 eV and 1044.52 eV corresponds to Zn 2p3/2 and Zn 2p1/2, which confirms that the Zn mainly exists in the form of $Zn^{2+}$ [30]. As for the N–ZnO NPs, the binding energy of Zn 2p3/2 shifts to a lower value, indicating the change of electronic structure of Zn. Differing from the reported doping ions such as $Bi^{3+}$, the N atoms can easily replace the oxygen atoms in ZnO crystal or enter into the lattice of ZnO crystal to form the Zn–N bonds, thus increasing the electron density of ZnO [31]. On the contrary, however, it is known that the N atoms could also occupy the oxygen vacancies in ZnO, decreasing the electron density of ZnO and then increasing the binding energy of $Zn^{2+}$. Here it can be proposed that the oxygen vacancies were eliminated before the N-doping process during thermal processing. As a result, the binding energy of $Zn^{2+}$ decreases in the N–ZnO NPs.

In comparison with the conventional solid-state process that usually involves high temperature combined with complicated steps, the fabrication of oxide semiconductor nanomaterials via the solution route is relatively mild. Among various chemical solution strategies, the solvothermal method has been widely improved to be an effective way to prepare low-dimensional nanostructures with precise control on morphology, structure, and dimension [32–35]. In this work, the ZnO NPs were successfully synthesized by the simple solvothermal route without using any surfactant. It is well-known that ZnO is crystallized by the hydrolysis of Zn salts that are formed using alkali compounds such KOH and NaOH [36]. The $Na^+$ ion, which has smaller ion radius than that of the $K^+$ ion, could be attracted by the $OH^-$ around the ZnO nanocrystals or nuclei and forms a capping layer, inhibiting the oriented growth of ZnO along the [0001] directions [37]. Finally, ZnO NPs rather than one-dimensional nanostructured ZnO were formed in this work. The main reactions involved in the formation of ZnO NPs are illustrated in the following conventional equations: $Zn^{2+}+OH^- \leftrightarrow Zn(OH)_2$, $Zn(OH)_2+2OH^- \leftrightarrow Zn(OH)_4^{2-}$, $Zn(OH)_4^{2-} \leftrightarrow ZnO+H_2O+2OH^-$ [38].

Based on the above discussions, the N atoms have been successfully incorporated into the ZnO NPs. The process of N-doping in the ZnO NPs with melamine as the N source could be explained as follows. Firstly, the melamine was transformed to isocyanic acid upon heating at 120 °C. When the temperature reached 380 °C, the isocyanic acid would be reacted with the residual $O_2$ or $H_2O$ in the chamber, leading to the formation of $NH_3$. Then, the $NH_3$ would be reacted with the ZnO NPs according to the following equations: $NH_3 \leftrightarrow NH^{2-}+2H^+$,

$ZnO + xNH^{2-} \leftrightarrow ZnO_{1-x}N_x + xH_2O$ [39]. After 2 h of reaction, the N-doped ZnO NPs were finally obtained. In addition, the melamine could be reacted with the $O_2$ and a small amount of $N_2$ was generated, further favoring the doping of N in the ZnO through the diffusion of N atoms. Interestingly, the remaining isocyanic acid can be reversibly transformed to melamine during the cooling process, which can be collected at both ends of the furnace for the next use. Although melamine is hazardous to health, no harmful by-product or impurity remained after the doping process and the reversibly-obtained melamine could be recycled, indicating that the present route for N doping is efficient and environmentally friendly.

The photocatalytic degradation of MO solutions under simulated sunlight was performed in order to investigate the photocatalytic properties of both the ZnO and the N–ZnO NPs. Fig. 4a shows the time course of MO degradation efficiencies over different photocatalysts. For comparison, MO degradation over $TiO_2$ NPs and N–$TiO_2$ under the same condition was simultaneously measured. In the case of undoped ZnO NPs and $TiO_2$ NPs, slightly photocatalytic performance was observed under simulated sunlight irradiation. Obviously, the photocatalytic activities of both the N–ZnO and the N–$TiO_2$ have been found to be better than that of the undoped ZnO and $TiO_2$, and the N–ZnO phtocatalyst produces the most effective photocatalytic activity among all the tested samples. The ultimate MO degradation efficiency over the N–ZnO photocatalyst is about 3.8 and 1.5 times higher than those over the ZnO and the N–$TiO_2$ photocatalysts, respectively. Fig. 4b shows that the absorbance of MO solution gradually decreased during the photodegradation under visible light irradiation by the N–ZnO NP photocatalyst. The maximum absorbance of the MO solution decreased abruptly from 0.8 (inset in Fig. 3b) to about 0.2 for 20 min irradiation, and the photodegradation efficiency is about ca. 80%. The adsorption peak corresponding to MO almost disappeared after about 100 min, indicating the excellent photocatalytic activity of the N–ZnO NPs.

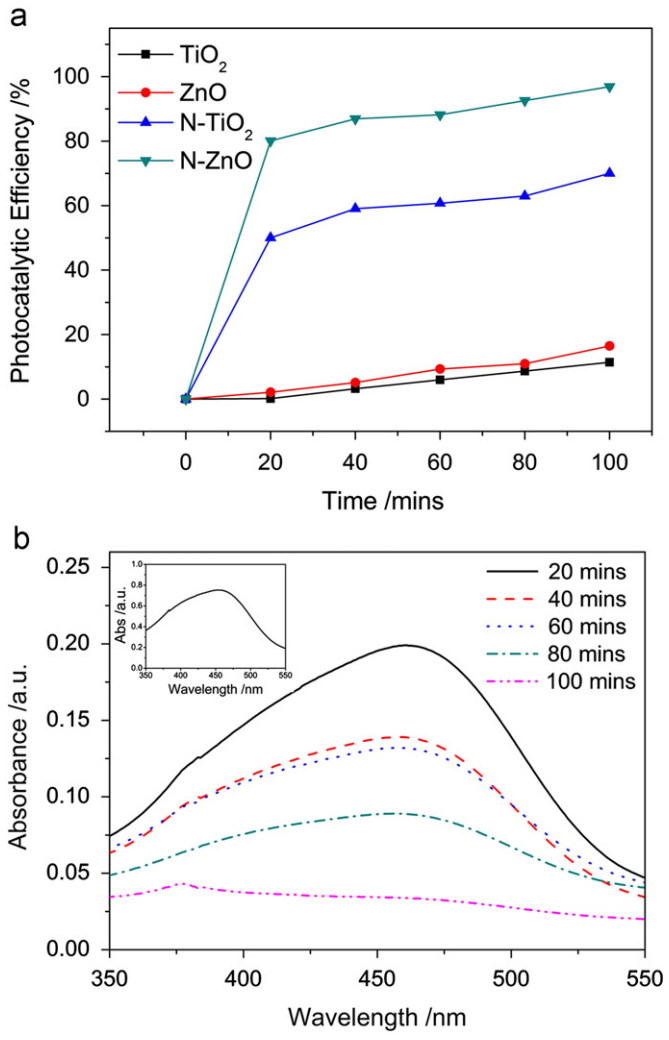


Fig. 4. (a) Time course of photodegradation efficiencies over different photocatalysts and (b) changing UV–vis spectrum for MO aqueous solution in the presence of N–ZnO NPs.

Oxide semiconductors, especially ZnO and $TiO_2$, have been widely investigated as photocatalysts for the degradation of organic pollutants. However, the wide bandgap of ZnO and $TiO_2$ restrict their photocatalytic applications to the ultraviolet (UV) region. The doping of ZnO and $TiO_2$ with nonmetals such as N, S, and F could increase their photocatalytic properties by extending their light absorption from the UV to the visible region [24–27]. The UV–vis diffuse reflectance spectra of the ZnO and N–ZnO NPs are shown in Fig. 5. It is obvious that the light-absorption edge of the N–ZnO NPs exhibits a slight red-shift towards the visible-light region with respect to that of the ZnO NPs. The bandgap of oxide semiconductors can be determined on the basis of the equation: $\alpha hv = A(hv - E_g)^n$, where $\alpha$ is absorption coefficient, $hv$ is the incident photon energy, $A$ is a constant, $n$ value is 1/2 for direct semiconductor [40]. According to the linear extrapolation of the plots of $(\alpha hv)^{1/2}$ vs $hv$, the bandgap are estimated to be 3.1 eV and 2.75 eV for the undoped and N-doped ZnO NPs, respectively. Namely, the N doping process yielded a 0.35 eV reduction in the bandgap of ZnO. The narrowing bandgap of N–ZnO should be attributed to the mixed O 2p and substitutional N 2p states or to the isolated N 2p

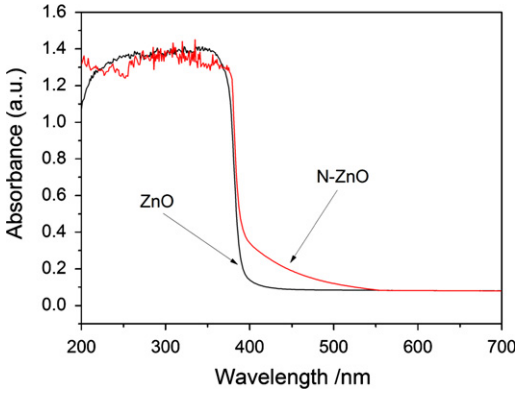


Fig. 5. UV–vis diffuse reflectance spectra of ZnO and N–ZnO NPs.

narrow band over the O 2p valence band [41,42]. Therefore, less energy is needed for the generation of charge carriers under light irradiation, i.e. photoexcited electrons ($e^-$) and holes ($h^+$). The electrons and holes could be reacted with $OH^-$ and absorbed $O_2$ to form the hydroxyl radicals ($OH^-$) and the superoxide radical anions ($O_2^-$), respectively, leading to the degradation of MO under visible-light irradiation [43]. In addition, the improved crystallinity of the N–ZnO NPs could suppress the recombination of the photoexcited electrons and holes, contributing equally to the improved photocatalytic properties. The improved photocatalytic activities of both the N–ZnO and the N–$TiO_2$ phtocatalysts have certainly verify the versatility of the present vacuum atmosphere method for preparing the N-doped oxide semiconductors.

## 4. Conclusions

We have developed a simple, rapid, and environmentally-friendly vacuum atmosphere method to prepare the N–ZnO NPs with the solvothermally-synthesized ZnO NPs as precursor and the melamine as N source. The present vacuum atmosphere method represents a new general route for preparing other N-doped oxide semiconductors such as $TiO_2$. Both the N–ZnO and the N–$TiO_2$ NPs were found to exhibit obviously improved photocatalytic performance for the degradation of methyl orange under simulated daylight irradiation in comparison with the undoped ZnO and $TiO_2$ NPs.

## Acknowledgment

This work is financially supported by the National Natural Science Foundation of China (Nos. 51202144 and 51202142), the Chenguang Scholar Project of Shanghai Education Commission (No. 11CG53), the Research and Innovation Project of Shanghai Education Commission (No. 12YZ113), and the Natural Science Foundation of Shandong (No. ZR2011EMQ011).

## Appendix A. Supporting information

Supplementary data associated with this article can be found in the online version at http://dx.doi.org/10.1016/j.ceramint.2012.12.018.

## References

[1] R.S. Devan, R.A. Patil, J.H. Lin, Y.R. Ma, One-dimensional metal-oxide nanostructures: recent developments in synthesis, characterization, and applications, Advanced Functional Materials 22 (2012) 3326–3370.

[2] R. Abe, Recent progress on photocatalytic and photoelectrochemical water splitting under visible light irradiation, Journal of Photochemistry and Photobiology C: Photochemistry Reviews 11 (2010) 179–209.

[3] H. Tong, S.X. Ouyang, Y.P. Bi, N. Umezawa, M. Oshikiri, J.H. Ye, Nano-photocatalytic materials: possibilities and challenges, Advanced Materials 24 (2011) 229–251.

[4] Y.C. Liao, C.S. Xie, Y. Liu, H. Chen, H.Y. Li, J. Wu, Comparison on photocatalytic degradation of gaseous formaldehyde by $TiO_2$, ZnO and their composite, Ceramics International 38 (2012) 4437–4444.

[5] Y.F. Hu, J. Zhou, P.H. Yeh, Z. Li, T.Y. Wei, Z.L. Wang, Supersensitive, fast-response nanowire sensors by using schottky contacts, Advanced Materials 22 (2010) 3327–3332.

[6] J. Zhao, L. Wang, X.Q. Yan, Y. Yang, Y. Lei, J. Zhou, Y.H. Huang, Y.S. Gu, Y. Zhang, Structure and photocatalytic activity of Ni-doped ZnO nanorods, Materials Research Bulletin 46 (2011) 1207–1210.

[7] H.C. Qin, W.Y. Li, Y.J. Xia, T. He, Photocatalytic activity of heterostructures based on ZnO and N-doped ZnO, ACS Applied Materials and Interfaces 3 (2011) 3152–3156.

[8] Y.R. Zhang, J. Wan, Y.U. Ke, A novel approach of preparing $TiO_2$ films at low temperature and its application in photocatalytic degradation of methyl orange, Journal of Hazardous Materials 177 (2010) 750–754.

[9] K. Shankar, J.I. Basham, N.K. Allam, O.K. Varghese, G.K. Mor, X.J. Feng, M. Paulose, J.A. Seabold, K.S. Choi, C.A. Grimes, Recent advances in the use of $TiO_2$ nanotube and nanowire arrays for oxidative photoelectrochemistry, Journal of Physical Chemistry C 113 (2009) 6327–6359.

[10] K. Nakata, A. Fujishima, $TiO_2$ photocatalysis: design and applications, Journal of Photochemistry and Photobiology C 13 (2012) 169–189.

[11] D.L. Chen, X.X. Hou, H.J. Wen, Y. Wang, H.L. Wang, X.J. Li, R. Zhang, H.X. Lu, H.L. Xu, S.K. Guan, J. Sun, L. Gao, The enhanced alcohol-sensing response of ultrathin $WO_3$ nanoplates, Nanotechnology 21 (2010) 035501.

[12] Z.G. Zhao, M. Miyauchi, Nanoporous-walled tungsten oxide nanotubes as highly active visible-light-driven photocatalysts, Angewandte Chemie-International Edition 47 (2008) 7051–7055.

[13] D. Vernardou, H. Drosos, E. Spanakis, E. Koudoumas, C. Savvakis, N. Katsarakis, Electrochemical and photocatalytic properties of $WO_3$ coatings grown at low temperatures, Journal of Materials Chemistry 21 (2011) 513–517.

[14] Y.D. Zhang, Z. Zheng, F.L. Yang, Highly sensitive and selective alcohol sensors based on Ag-doped $In_2O_3$ coating, Industrial and Engineering Chemistry Research 49 (2010) 3539–3543.

[15] Z.Z. Han, L. Liao, Y.T. Wu, H.B. Pan, S.F. Shen, J.Z. Chen, Synthesis and photocatalytic application of oriented hierarchical ZnO flower-rod architectures, Journal of Hazardous Materials 217–218 (2012) 100–106.

[16] K. Hirota, M. Sugimoto, M. Kato, K. Tsukagoshi, T. Tanigawa, H. Sugimoto, Preparation of zinc oxide ceramics with a sustainable antibacterial activity under dark conditions, Ceramics International 36 (2010) 497–506.

[17] X.D. Wang, J.H. Song, J. Liu, Z.L. Wang, Direct-current nanogenerator driven by ultrasonic waves, Science 316 (2007) 102–105.

[18] Z.L. Wang, Self-powered nanosensors and nanosystems, Advanced Materials 24 (2012) 280–285.

[19] A. Abdolmaleki, S. Mallakpour, S. Borandeh, The use of novel biodegradable, optically active and nanostructured poly (amide–ester–imide) as a polymer matrix for preparation of modified ZnO based bionanocomposites, Materials Research Bulletin 47 (2012) 1123–1129.

[20] R. Hariharan, S. Senthikumar, A. Suganthi, M. Rajarajan, Synthesis and characterization of doxorubicin modified ZnO/PEG nanomaterials and its photodynamic action, Journal of Photochemistry and Photobiology B 116 (2012) 56–65.

[21] Y. Zheng, L. Zheng, Y. Zhan, X. Lin, Q. Zheng, K. Wei, Ag/ZnO heterostructure nanocrystals: synthesis, characterization, and photocatalysis, Inorganic Chemistry 46 (2007) 6980–6986.

[22] M. Zheng, J.Q. Wu, One-step synthesis of nitrogen-doped ZnO nanocrystallites and their properties, Applied Surface Science 255 (2009) 5656–5661.

[23] T.C. Jagadale, S.P. Takale, R.S. Sonawane, H.M. Joshi, S.I. Patil, B.B. Kale, S.B. Ogale, N-doped tio$_2$ nanoparticle based visible light photocatalyst by modified peroxide sol–gel method, Journal of Physical Chemistry C 112 (2008) 14595–14602.
[24] S.S. Shinde, C.H. Bhosale, K.Y. Rajpure, Photocatalytic degradation of toluene using sprayed N-doped ZnO thin films in aqueous suspension, Journal of Photochemistry and Photobiology B 113 (2012) 70–77.
[25] A.B. Patil, K.R. Patil, S.K. Pardeshi, Ecofriendly synthesis and solar photocatalytic activity of S-doped ZnO, Journal of Hazardous Materials 183 (2010) 315–323.
[26] X.Y. Yang, A. Wolcott, G.M. Wang, A. Sobo, R.C. Fitzmorris, F. Qian, J.Z. Zhang, Y. Li, Nitrogen-doped ZnO nanowire arrays for photoelectrochemical water splitting, Nano Letters 9 (2009) 2331–2336.
[27] Y.C. Qiu, K.Y. Yan, H. Deng, S.H. Yang, Secondary branching and nitrogen doping of ZnO nanotetrapods: building a highly active network for photoelectrochemical water splitting, Nano Letters 12 (2012) 407–413.
[28] G.Z. Shen, J.H. Cho, J.K. Yoo, G.C. Yi, C.J. Lee, Synthesis and optical properties of S-doped ZnO nanostructures: nanonails and nanowires, Journal of Physical Chemistry B 109 (2005) 5491–5496.
[29] L.J. Luo, W. Tao, X.Y. Hu, T. Xiao, B.J. Heng, W. Huang, H. Wang, H.W. Han, Q.K. Jiang, J.B. Wang, Y.W. Tang, Mesoporous F-doped ZnO prism arrays with significantly enhanced photovoltaic performance for dye-sensitized solar cells, Journal of Power Sources 196 (2011) 10518–10525.
[30] S.S. Shinde, K.Y. Rajpure, Fabrication and performance of N-doped ZnO UV photoconductive detector, Journal of Alloys and Compounds 522 (2012) 118–122.
[31] J.B. Zhong, J.Z. Li, Y. Lu, X.Y. He, J. Zeng, W. Hu, Y.C. Shen, Fabrication of Bi3+-doped ZnO with enhanced photocatalytic performance, Applied Surface Science 258 (2012) 4929–4933.
[32] J.G. Yu, X.X. Yu, Hydrothermal synthesis and photocatalytic activity of zinc oxide hollow spheres, Environmental Science and Technology 42 (2008) 4902–4907.
[33] X.T. Chang, S.B. Sun, Y. Zhou, L.H. Dong, Y.S. Yin, Solvothermal synthesis of Ce-doped tungsten oxide nanostructures as visible-light-driven photocatalysts, Nanotechnology 22 (2011) 265603.
[34] S.H. Ko, D. Lee, H.W. Kang, K.H. Nam, J.Y. Yeo, S.J. Hong, C.P. Grigoropoulos, H.J. Sung, Nanoforest of hydrothermally grown hierarchical ZnO nanowires for a high efficiency dye-sensitized solar cell, Nano Letters 11 (2011) 666–671.
[35] J.H. Tian, J. Hu, S.S. Li, F. Zhang, J. Liu, J. Shi, X. Li, Z.Q. Tian, Y. Chen, Improved seedless hydrothermal synthesis of dense and ultralong ZnO nanowires, Nanotechnology 22 (2011) 245601.
[36] S. Xu, Z.L. Wang, One-dimensional ZnO nanostructures: solution growth and functional properties, Nano Research 4 (2011) 1013–1098.
[37] R. Viswanatha, H. Amenitsch, D.D. Sarma, Growth kinetics of ZnO nanocrystals: a few surprises, Journal of the American Chemical Society 129 (2007) 4470–4475.
[38] L.N. Dem'yanets, D.V. Kostomarov, I.P. Kuz-mina, Chemistry and kinetics of ZnO growth from alkaline hydrothermal solutions, Inorganic Materials 38 (2002) 124–131.
[39] H.Y. Wei, Y.S. Wu, L.L. Wu, C.X. Hu, Preparation and photoluminescence of surface N-doped ZnO nanocrystal, Materials Letters 59 (2005) 271–275.
[40] D. Chen, L. Gao, A. Yasumori, K. Kuroda, Y. Sugahara, Size- and shape-controlled conversion of tungstate-based inorganic–organic hybrid belts to $WO_3$ nanoplates with high specific surface areas, Small 4 (2008) 1813–1822.
[41] M. Batzill, E.H. Morales, U. Diebold, Influence of nitrogen doping on the defect formation and surface properties of $TiO_2$ rutile and anatase, Physical Review Letters 96 (2006) 026103.
[42] H. Irie, Y. Watanabe, K. Hashimoto, Nitrogen-concentration dependence on photocatalytic activity of $TiO_{2-x}N_x$ powders, Journal of Physical Chemistry B 107 (2003) 5483.
[43] F.H. Chu, C.W. Huang, C.L. Hsin, C.W. Wang, S.Y. Yu, P.H. Yeh, W.W. Wu, Well-aligned ZnO nanowires with excellent field emission and photocatalytic properties, Nanoscale 4 (2011) 1471–1475.